



**HAL**  
open science

# Influence of Temporal Parameters of DCE-MRI on the Quantification of Heterogeneity in Tumor Vascularization

Amandine Crombé, Olivier Saut, Jerome Guigui, Antoine Italiano, Xavier  
Buy, Michèle Kind

► **To cite this version:**

Amandine Crombé, Olivier Saut, Jerome Guigui, Antoine Italiano, Xavier Buy, et al.. Influence of Temporal Parameters of DCE-MRI on the Quantification of Heterogeneity in Tumor Vascularization. *Journal of Magnetic Resonance Imaging*, 2019, 50 (6), pp.1773-1788. 10.1002/jmri.26753 . hal-02406497

**HAL Id: hal-02406497**

**<https://inria.hal.science/hal-02406497>**

Submitted on 13 Dec 2019

**HAL** is a multi-disciplinary open access archive for the deposit and dissemination of scientific research documents, whether they are published or not. The documents may come from teaching and research institutions in France or abroad, or from public or private research centers.

L'archive ouverte pluridisciplinaire **HAL**, est destinée au dépôt et à la diffusion de documents scientifiques de niveau recherche, publiés ou non, émanant des établissements d'enseignement et de recherche français ou étrangers, des laboratoires publics ou privés.

## TITLE

# Influence of Temporal Parameters of DCE-MRI on the Quantification of Heterogeneity in Tumor Vascularization.

[Cromb  A](#)<sup>1,2</sup>, [Saut O](#)<sup>2</sup>, [Guigui J](#)<sup>1</sup>, [Italiano A](#)<sup>3</sup>, [Buy X](#)<sup>1</sup>, [Kind M](#)<sup>1</sup>.

1. Department of Radiology, Institut Bergoni , Comprehensive Cancer Center, Bordeaux, France.
2. University of Bordeaux, IMB, UMR CNRS 5251, INRIA Project Team Monc, Talence, France.
3. Department of Medical Oncology, Institut Bergoni , Comprehensive Cancer Center, Bordeaux, France.

## ABSTRACT:

**Background:** Evaluating heterogeneity in tumor vascularization through texture analysis could improve predictions of patients' outcome and response evaluation.

**Purpose:** To investigate the influence of temporal parameters on texture features extracted from DCE-MRI parametric maps.

**Study type:** Prospective cross-sectional study

**Subjects:** 25 adults with soft-tissue sarcoma (STS), median age: 68 years.

**Field Strength/Sequence:** DCE-MRI acquisition using a CAIPIRINHA-Dixon-TWIST-VIBE sequence at 1.5T (temporal resolution: 2s, duration: 5min).

**Assessment:** The area under time-intensity curve (AUC) and  $K^{trans}$  maps were generated for several temporal resolution (dt=2s, 4s, 6s, 8s, 10s, 12s, 20s) and scan durations (T=3min, 4min, 5min for a 6s-sampling) by downsampling and truncating the initial DCE-MRI sequence. Tumor volume was manually segmented and propagated on all parametric maps. Thirty-two first- and second order-texture features were extracted per map to quantify the intra-tumoral heterogeneity.

**Statistical Tests:** The influence of temporal parameters on texture features was studied with repeated-measures ANOVA (or non-parametric equivalent). The dispersion of each texture feature depending on temporal parameters was estimated with coefficients of variation (CV). The performances of multivariate models to predict the response to chemotherapy (i.e. binary logistic regression based on the baseline texture features) were compared.

**Results:** The temporal resolution had a significant influence on 12/32 (37.5%) and 14/32 (43.8%) texture features evaluated on AUC and  $K^{\text{trans}}$  maps, respectively (range of p-values: <0.0001-0.0395). Scan duration had a significant influence on 23/32 (71.9%) texture features from  $K^{\text{trans}}$  map (range of p-values: <0.0001-0.0321). Dispersion was high (: mean CV>0.5) with sampling for 2/32 (6.3%) and 10/32 (31.3%) features from AUC and  $K^{\text{trans}}$  maps, respectively; and with truncating for 6/32 (18.8%) features from  $K^{\text{trans}}$  map. The AUROC of predictive models ranged from 0.77 (CI95%=[0.54-1.00], with dt=6s-T=4min) to 0.90 (CI95%=[0.74-1.00], with dt=6s-T=5min).

**Data Conclusion:** The values of texture features extracted from DCE-MRI parametric maps can be influenced by temporal parameters, which can lead to variations in performances of predictive models.

**Level of evidence:** 2

**Technical efficacy:** 2

## KEYWORDS

Radiomics; Texture analysis; oncology; DCE-MRI; Sarcoma; Sequence optimization

## ABBREVIATIONS

AIF: Arterial input function

AUC: Area under curve

AUROC: Area under the receiver operating characteristics curve

CI95%: 95% confidence interval

CV: Coefficient of variation

DCE-MRI: Dynamic contrast-enhanced MRI

FNCLCC: French *Federation Nationale des Centres de Lutte Contre le Cancer*

FOS: First order statistics

GL: Grey level

GLCM: Grey level occurrence matrix

GLRLM: Grey level run-length matrix

GLSZM: Grey level size zone matrix

$K^{\text{trans}}$ : Influx volume transfer constant

QIBA®: Quantitative Imaging Biomarkers Alliance

rm: Repeated measures

SD: standard deviation

STS: soft-tissue sarcomas

TSE: turbo spin echo

VIBE: Volume interpolated breath-hold examination

VOI: Volume of interest

## INTRODUCTION

The extensive quantification of tumor heterogeneity on medical imaging is a growing field of research in oncology referred to as radiomics. The underlying hypothesis of radiomics is that the imaging phenotype of a tumor could reflect its intrinsic molecular identities and aggressiveness (1, 2). Texture analyses consist in the mathematical processing of images in order to extract numeric indices that objectively measure the heterogeneity, named texture features. The most commonly encountered ones in the medical literature are 1<sup>st</sup> order features, which are based on frequency histograms without spatial information, and 2<sup>nd</sup> order features, which quantify the 2D and/or 3D rearrangements of voxels of different gray-levels. Predictive radiomics approaches based on texture features, machine learning algorithms and the potential combination with clinical characteristics and other –omics data (i.e. genomics, transcriptomics, proteomics and metabolomics) could help better stratify the therapeutic strategy for cancer patients and evaluate treatment responses (2).

Radiomics approaches can be applied to every imaging modality including dynamic contrast-enhanced MRI (DCE-MRI). DCE-MRI aims at providing a non-invasive macroscopic assessment of tumor perfusion and neo-angiogenesis – a key pro-oncogenic process – through the rapid acquisition of a time series of T1-weighted imaging (3). DCE-MRI parameters have been used to discriminate benign from malignant tumors or to monitor treatment efficacy especially anti-angiogenic regimens – the area under the time intensity curve (AUC) and the influx volume transfer constant ( $K^{\text{trans}}$ ) being the most studied) (4) . However, these studies were based on average values of the DCE-MRI parameters that do not reflect the complexity of tumors. Indeed, homogeneous poorly vascularized tumors could have the same mean AUC and  $K^{\text{trans}}$  values as heterogeneous tumors with both hypervascularized and large avascular necrotic areas. Consequently, quantifying the spatial heterogeneity in vascularization of the whole tumor volume from DCE-MRI data may be more informative and realistic. In that sense, radiomics approaches on DCE-MRI have recently shown encouraging results, alone or with other MRI sequences, in order to improve the detection of prostate cancer, to distinguish benign and malignant adnexal masses, to identify relevant molecular subtypes of breast cancers, to detect lymph node metastases in breast cancers, or to predict response to neoadjuvant treatment for rectum, breast and nasopharyngeal cancers (5–12) . Soft-tissue sarcomas (STS) are malignant mesenchymal tumors with important inter and

intra-tumoral heterogeneity known to be associated with high grade (13). Previous studies have shown that DCE-MRI could be useful to predict response to chemotherapy in high-grade STS (14–17), as well as radiomics approaches (16, 18, 19). Thus, it can be hypothesized that combining radiomics and DCE-MRI could enhance the early prediction of tumor response to treatment.

Robust radiomics models require the inclusion of a large number of patients, divided into training, validation and external test cohorts, before being implemented into clinical practice. Pooling data from different centers is necessary but it runs the risk of introducing bias to the values of texture features. Indeed, each step of the radiomics process can introduce variability independently from the intrinsic heterogeneity of the tumor, for instance: MRI field strength, manufacturers, coils, acquisition parameters, segmentation, voxel-size resampling, normalization techniques or grey-level discretization (20–23). Previous studies have demonstrated that temporal parameters (i.e. scan duration and temporal resolution) could significantly modify the ability to discriminate benign from malignant prostate or breast lesions (24–26), but they were based on average values of DCE-MRI indices or morphology of the time-intensity curves. Only one study has focused on the stability of texture features extracted from computed tomography perfusion maps identifying an influence of temporal resolution (27). Hence, data regarding the influence of temporal parameters on texture features extracted from DCE-MRI parametric maps are lacking.

Thus, our aims were to investigate the influence of temporal parameters: (i) on the values of widely used texture features extracted from DCE-MRI parametric maps of STS, (ii) on the dispersion of these parameters, and (iii) on the performance of predictive models for chemotherapy responses.

## **MATERIALS AND METHODS**

### ***Patient population***

In this prospective single-center study, the institutional review board waived the requirements of informed patient consent. From November 2017 to June 2018, 30 consecutive adult patients were included as they presented at our sarcoma reference center for the management of a histologically-proven high-grade (according to the French *Federation Nationale des Centres de Lutte contre le Cancer* [FNCLCC] grading system) STS of the trunk wall or extremities of more than 4cm, and required a contrast-enhanced MRI for diagnostic and/or therapeutic management. Age, gender, histological type, tumor depth relative to superficial fascia, tumor location, longest diameter, specific treatments and short-term patients' outcome were retrieved from medical records. We defined a good responder as: (i) <10% of stainable viable tumor cells on surgical specimen after neo-adjuvant chemotherapy for locally-advanced non-metastatic STS (28), and (ii) a partial or complete response 6 months after performing DCE-MRI according to RECIST 1.1 criteria for metastatic or inoperable patients, without changing treatment – this last empirical definition being proposed regarding the usual median progression-free survivals of metastatic STS patients (29).

### ***Data acquisition***

Patients underwent MRI scans in the same 1.5T MR-system (MAGNETOM Aera; Siemens Healthineers, Erlangen, Germany) with adapted coils depending on tumor locations and sizes, i.e. 15 channels transmit/receiver coil for knee and extremities and 18 channels transmit/receiver body coil for trunk wall and thighs. Patients were examined in supine position. The protocol followed the Quantitative Imaging Biomarkers Alliance recommendations (QIBA®) and consisted in a T1-mapping followed by the DCE-MRI acquisition with the same field-of-view (350 x 320 mm) and spatial resolution (1.1 x 1.1 x 4 mm<sup>3</sup>), in order to optimize the conversion of the signal in Gadolinium chelates concentration. We used a CAIPIRINHA (Controlled Aliasing in Parallel Imaging Results in Higher Acceleration) Dixon TWIST (Time-resolved angiography With Stochastic Trajectories) VIBE (Volume Interpolated Breath hold Examination) sequence (30). The T1-mapping used a similar spoiled gradient-echo sequence with variable flip angles (2° and 15°) and with echo and repetition times of 1.41ms and 3.79ms, respectively. In brief, the principle of TWIST

is to divide the k-space in a central region, which encodes information about contrast, and a peripheral region, which encodes information about shapes, edges and details and is undersampled (30). The suppression of the fat signal was performed using a Dixon-based water-fat separation (echo times were 2.39ms for in-phase and 4.77ms for opposite-phase conditions). A repetition time of 6.89ms and a flip angle of 25° were used. The sampling was accelerated with a parallel acquisition technique with an undersampling factor of 2. The value of the TWIST view-sharing parameters A (i.e. the percentage sizes of the central portion of the k-space) and B (i.e. the percentage sizes of the peripheral portion of the k-space) were 15% and 20%, respectively. The temporal resolution resulted in  $dt=2s$ , except for the first TWIST phase (6.9s for the full k-space sampling). Five phases were acquired before the intra-venous power-injection of 0.1mmol/kg of gadoteric acid (Dotarem, Guerbet, Villepinte, France) at a rate of 2mL/s followed by a 20mL flush of 0.9% of NaCl solution thanks to a MRI-compatible automatic injector (Sonic Shot 7, Nemoto Kyorindo, Tokyo, Japan). The total scan duration was 5min and included 144 phases (full-dataset).

### ***Data reconstruction***

Data reconstruction and post-processing were achieved with Olea Sphere®, v3.0 SP14 Software (Olea Medical, La Ciotat, France) by a senior radiologist with 7 years of experience in MRI blinded to clinical data. First, motion artifacts were systematically corrected with a rigid body co-registration method. For each patient, the full-dataset was downsampled and truncated to obtain the datasets to assess the effect of scan duration and temporal resolution. In any case, the 5 first phases were kept in the datasets to ensure a similar baseline for all maps. In total, 7 DCE-MRI datasets per patient were generated to evaluate temporal resolution, namely:  $dt=2s$  (raw data), 4s, 6s, 8s, 10s, 12s, 20s, with a scan duration of 5min. Three DCE-MRI datasets were generated to evaluate the influence of scan duration, namely: T=3min, 4min, 5min, all with a temporal resolution of  $dt=6s$ . Figure 1 shows how the datasets were built.

The next step consisted in the calculation of the parametric maps using the permeability plug-in of Olea Sphere®. First, the senior radiologist manually chose the largest feeding artery within the field-of-view of the raw DCE-MRI dataset, with the exclusion of the first and the last slices to avoid artifacts. A fixed voxel was manually placed in this artery and the arterial input function (AIF) was measured as the average

of 4 directly adjacent voxels within this artery that demonstrated an arterial enhancement and the less noise. The same artery and the same voxels were used for the other reconstructed datasets. Hence, even if the baseline of the AIF was preserved, the AIF was also downsampled and truncated (Fig. 1). Second, the AIF signal intensity time-course was converted into blood R1 time-course, with the hematocrit = 0.45 and the gadoteric acid relaxivity at 1.5T = 3.6 L/mmol.s<sup>-1</sup>. We chose to focus on the most widely used parameters: the area under the time-intensity curve (AUC), at 90s (units: mmol/L/s) and the pharmacokinetic parameter K<sup>trans</sup> (influx volume transfer constant from plasma to extra-vascular, extracellular space, which represents the capillary permeability, units: min<sup>-1</sup>). K<sup>trans</sup> maps were calculated using the Extended Tofts model (31). Of note, AUC was not evaluated for scan duration because we focused on the first 90 seconds of the time-intensity curve.

Five out of the 30 MRI examinations were excluded due to Dixon fat-water swap artifacts (n=3) and motion artifacts (that were too large to be well corrected with the motion correction, n=2) biasing the quantitative assessment.

### ***Data analysis***

*Texture analysis.* For each patient, the entire tumor volume was manually segmented by the same senior radiologist using OleaSphere®, slice-by-slice, on the last phase of the DCE-MRI acquisition (because the tumor demonstrated the best contrast with surrounding tissues compared with the other phases) and with the help of the conventional sequences acquired during the same MRI examination, i.e.: axial turbo spin echo (TSE) T2-weighted imaging (refocusing angle = 150°, repetition time = 6860ms, echo time = 120ms, slice thickness = 4mm, field-of-view = 250 x 250mm), coronal or sagittal TSE short time inversion recovery T2-weighted imaging (refocusing angle = 150°, repetition time = 4150ms, echo time = 69ms, inversion time = 150ms, slice thickness = 4mm, field-of-view = 350 x 350mm), axial TSE T1-weighted imaging (refocusing angle = 150°, repetition time = 420ms, echo time = 10ms, slice thickness = 4mm, field-of-view = 250 x 250mm), pre- and post-contrast agent injection axial Fat-Sat TSE T1-weighted imaging (refocusing angle = 180°, repetition time = 581ms, echo time = 10ms, slice thickness = 4mm, field-of-view = 250 x 250mm). The voxels located at the extreme edge of the tumor were excluded to avoid partial volume effect. The volume of interest (VOI) was then propagated on all the parametric maps (K<sup>trans</sup> and AUC for the 7 samplings, K<sup>trans</sup> for the 3 truncations).

Texture analysis consisted in the 3D extraction of 32 quantitative features, provided in Table 1, from histogram analysis (: first order statistics, FOS), grey-level co-occurrence matrix (GLCM), grey-level run-length matrix (GLRM) and grey-level size zone matrix (GLSZM) (32–34). Before,  $K^{\text{trans}}$  and AUC values were discretized in 256 bins. The spatial offset was fixed to a displacement of 4 pixels and an angle of  $45^\circ$  (details regarding the definitions and calculations of the texture features are given in Supplementary Data 1). No technique for resampling or standardization was applied because the voxel size was initially the same for all patients and texture analysis was performed on scaled parametric maps and not on raw MRI data.

For each patient ‘p’ ( $i \in \{1;2;\dots;N_p\}$  where  $N_p$  is the total number of included patients), for each feature ‘ $F_i$ ’ ( $i \in \{1;2;\dots;32\}$ ) and for each DCE-MRI map ‘X’ ( $X \in \{K^{\text{trans}}; \text{AUC}\}$ ), we extracted 7 paired values of  $F_{p,i,X}$  regarding sampling and 3 paired values of  $F_{p,i,X}$  regarding scan duration ( $F_{p,i,X}(\text{dt})$  and  $F_{p,i,X}(T)$ , respectively).

*Coefficient of variation (CV)*. We calculated the mean CV and its standard deviation (SD) on each feature  $F_i$  in order to assess the influence of sampling (: CV-dt, with AUC or  $K^{\text{trans}}$ ), and scan duration (: CV-T, with  $K^{\text{trans}}$ ) on the dispersion of the texture features, as follows:

$$\text{CV-dt} = \sum_{p=1}^{N_p} (\text{SD}(F_{i,p,\text{dt}2}; F_{i,p,\text{dt}4}; \dots; F_{i,p,\text{dt}20}) / \text{mean}(F_{i,p,\text{dt}2}; F_{i,p,\text{dt}4}; \dots; F_{i,p,\text{dt}20})) / N_p$$

$$\text{CV-T} = \sum_{p=1}^{N_p} (\text{SD}(F_{i,p,T3}; F_{i,p,T4}; ; F_{i,p,T5}) / \text{mean}(F_{i,p,T3}; F_{i,p,T4}; F_{i,p,T5})) / N_p$$

We defined a texture feature as very poorly variable if  $\text{CV} < 0.1$ , poorly variable if  $\text{CV} \in [0.1-0.2[$ , mildly variable if  $\text{CV} \in [0.2-0.5[$ , highly variable if  $\text{CV} \in [0.5-1[$  and extremely variable if  $\text{CV} \geq 1.0$ .

### ***Statistical analysis***

Statistical analyses were performed using SPSS (IBM corp, version 21.0, Armonk, NY) and GraphPad Prism (GraphPad Software, version 7, San Diego, CA). Variables were expressed as average, standard deviation, median, and range, as appropriate. A p-value  $< 0.05$  was deemed significant. All tests were two-tailed.

Normality was assessed for each continuous value by using the Shapiro-Wilk test.

Repeated-measures (rm-) ANOVA with Geisser-Greenhouse correction for non-sphericity and post-hoc Tukey tests with corrections for multiple comparisons using statistical hypothesis testing (or non-parametric equivalent rm-Friedman tests with

post-hoc Dunn tests) were used to study the influence of sampling and truncating on texture features extracted from  $K^{\text{trans}}$  and AUC maps.

For texture features with a statistical influence of temporal resolution, a linear model was applied for correlation analysis. A Bonferroni correction was applied for multiple comparisons and a p-value of 0.01 was considered significant.

Finally, we investigated the influence of temporal parameters on the performance of a model aiming at predicting the treatment response based on texture features from  $K^{\text{trans}}$  and AUC maps. Twenty patients were analyzable for this part of the study; the 5 others were either operated directly after the MRI without chemotherapy or were not sufficiently followed-up. Texture features that were associated with the response at univariate level according to Student t-tests (or Mann-Whitney tests) with a p-value  $<0.05$  were entered in a multivariate binary logistic regression using a backward stepwise selection method based on the probability of the Wald statistics. The area under the receiver operating characteristics curve (AUROC) of the models were calculated according to scan durations and temporal resolutions and compared according to the Delong methods (35).

## RESULTS

### *Patients (Table 2)*

Twenty-five patients were finally included (9/25 (36%) women, median age 68 years old, range: 31-94). The most frequent histotype was undifferentiated pleomorphic sarcoma. The median size was 81mm (range: 42-180) and the median tumor volume was 0.357L (range: 0.023 – 1.048).

### *Influence of temporal parameters on DCE-MRI texture features*

Table 3 provides the results of the rm-ANOVA (or rm-Friedman test). Regarding the effect of temporal resolution, 12/32 (37.5%) AUC-based texture features were significantly influenced: 5/7 FOS features, 1/9 GLCM features, 2/9 GLRLM features and 4/7 GLSZM features (range of p-value=0.0395 to <0.0001). Fourteen out of 32 (43.8%)  $K^{\text{trans}}$ -based texture features were significantly influenced by temporal resolution: 1/7 FOS features, 5/9 GLCM features, 4/9 GLRLM features and 4/7 GLSZM features (range of p-value=0.0331 to 0.0007).

Regarding the effect of scan duration, 23/32 (71.9%)  $K^{\text{trans}}$ -based texture features were significantly influenced: 7/7 FOS features, 8/9 GLCM features, 6/9 GLRLM features and 2/7 GLSZM features (range of p-value=0.0321 to <0.0001).

Three texture features were influenced by temporal parameters in the 3 settings: GLRLM\_GL\_Variance, GLSZM\_Large\_area\_emphasis, and GLSZM\_Zone\_variance. Six texture features were not, no matter the setting: GLCM\_Correlation, GLRLM\_Gray\_level\_non-uniformity, GLRLM\_Run\_entropy, GLRLM\_Run\_variance, GLSZM\_Small\_area\_emphasis and GLSZM\_Zone\_entropy.

A summary of post-hoc tests is given in Table 4. Regarding the influence of temporal resolution on AUC maps, the highest number of texture features that statistically differed was observed in post-hoc comparisons between dt=20s and dt=2s (10/32, 31.3%) and dt=20s and dt=4s (9/32, 28.1%). On  $K^{\text{trans}}$  maps, the highest differences were seen between dt=20s and dt=2s (10/32, 59.4%), followed by dt=20s versus dt=6s (6/32, 18.8%). Regarding the influence of truncating on  $K^{\text{trans}}$  maps, 23/32 (71.9%) and 17/32 (53.1%) texture features were significantly different between T=5min and T=4min, and between T=5min and T=3min, respectively.

Significant linear correlations were found between sampling on AUC and GLSZM\_Size\_zone\_non-uniformity ( $p=0.0018$ ,  $r^2=0.879$ ) and GLSZM\_Zone\_variance ( $p=0.0043$ ,  $r^2=0.830$ ). Similarly, there were significant linear

correlations between sampling on  $K^{\text{trans}}$  and 4 texture features: GLSZM\_non-uniformity ( $p < 0.0001$ ,  $r^2 = 0.978$ ), GLSZM\_Large area emphasis ( $p = 0.0009$ ,  $r^2 = 0.909$ ), GLSZM\_Size\_zone\_non-uniformity ( $p = 0.0002$ ,  $r^2 = 0.954$ ), GLSZM\_Zone\_variance ( $p = 0.0002$ ,  $r^2 = 0.950$ ) (Fig. 2). Variations in scan duration did not reveal any linear correlations. Details for linear regressions are given in Supplementary Data 2. Figure 3 shows an example of variation of parametric maps and corresponding histograms with changes in scan duration and temporal resolution.

### ***Effect of temporal parameters on the dispersion of DCE-MRI texture features***

Figure 4 and Table 5 summarize the analysis of dispersion of texture features according to the 3 configurations (i.e. AUC-sampling,  $K^{\text{trans}}$ -sampling,  $K^{\text{trans}}$ -truncating). Most texture features extracted from AUC maps remained poorly to mildly variable with changes in sampling. Only GLCM\_Cluster\_prominence was categorized as highly variable ( $CV\text{-}dt = 0.50$ ), while 11 out of 32 (34.4%) texture features extracted from  $K^{\text{trans}}$  were highly to extremely variable (range of  $CV\text{-}dt = 0.50\text{-}1.11$ ).

Five texture features extracted from  $K^{\text{trans}}$  maps were highly variable with changes in scan duration: FOS\_Average, FOS\_Energy, FOS\_Inter-quartile\_range, FOS\_Standard\_deviation and GLSZM\_Zone\_entropy (range of  $CV\text{-}T = 0.54\text{-}0.96$ ). Supplementary Data 3 provides all the values of CV with SD.

### ***Effect of temporal parameters on a prediction based on DCE-MRI texture features***

Twenty patients were treated with chemotherapy and were analyzable for this sub-part of the study. There were 5/20 (25%) good responses (4 good histological responses and 1 partial response after 6 months without changing treatment). Table 6 shows the results of univariate analyses and performances of the models quantified by AUROC. After univariate analyses, the selected variables entered in the binary logistic regression were not systematically the same when temporal resolution and scan duration changed, even if some were frequently encountered: AUC\_GLRM\_Run\_entropy (in 8 models),  $K^{\text{trans}}$ \_GLSZM\_Small\_area\_emphasis (in 3 models). AUROC ranged from 0.77 ( $CI_{95\%} = (0.54\text{-}1.00)$ ) with a scan duration of 5min and a temporal resolution of 6s, to 0.90 ( $CI_{95\%} = (0.74\text{-}1.00)$ ) with a scan duration of 4min and a temporal resolution of 6min. Details of the univariate analyses

for each model and comparisons between AUROC can be found in Supplementary Data 4 and Supplementary Data 5, respectively.

## DISCUSSION

In this study, we examined the influence of temporal parameters on a large set of widely used and easily available statistical texture features extracted from whole tumor volumes segmented on  $K^{\text{trans}}$  and AUC parametric maps. We found that a large number of them were significantly dependent on the scan duration and temporal resolution. Moreover, merely half of them remained poorly variable with changes in temporal parameters. This led to non-negligible variations in the AUROCs of the models for a response prediction to chemotherapy, even though the comparisons did not provide statistical differences.

A major challenge for radiomics approaches is to ensure a good quality of the quantitative data on which they rely. Besides reproducibility, repeatability, non-redundancy and validity, quality here means controlling the bias due to slight variations in the imaging acquisition parameters (2). Standardizing the imaging protocols between radiological centers is unavoidable. However, thousands of MRI examinations (and DCE-MRI sequences) have already been acquired and the temptation to pool data from different MR-systems in order to begin to build and test predictive models for key oncological questions is understandable. Our study focused on STS as a tumor model to examine the influence of temporal parameters. High-grade STS are characterized by complex architectures and changes during treatments, making them particularly appropriate for radiomics. In particular, Vallières *et al.* stressed the influence of the post-processing parameters of imaging on a prediction model of occurrence of lung metastases in STS patients (36).

Our results are in agreement with previous studies that investigated the influence of temporal parameters on dynamic acquisitions. Othman *et al.* showed that shorter scan duration was responsible for overestimation of pharmacokinetic parameters and lead to incorrect classifications of benign prostate lesions as malignant (24). A similar influence on prediction models was found with breast lesions (26). This could be explained by the Tofts model itself because it assumes an immediate equilibrium between the compartments though it requires up to 2min in case of breast imaging (37). Poor temporal resolutions can also lead to incorrect assessments of pharmacokinetic parameters according to pre-clinical and clinical studies regarding prostate lesions – even if it did not significantly modify the ability of these parameters to discriminate benign and malignant tumors (25). Heisen *et al.* showed that the  $K^{\text{trans}}$

variations could go up to 25% of its initial value with varying temporal resolutions (38). In the single study that focused on the acquisition parameters at risk of influencing perfusion maps, Bogowicz *et al.* found that the percentage of unstable texture features ranged from 56 to 98% with different artery contouring, and from 58 to 75% with different temporal resolution, which is higher than in our study (27). This highest variability in their study may be explained by the difference in histological types, in imaging modality (CT vs. MRI), in the texture features that were calculated and in the perfusion maps that were studied (blood flow, mean time transit and blood volume vs. AUC and  $K^{\text{trans}}$  in our studies).

Regarding STS, our results also highlight potential cut-offs for temporal resolution and scan duration beyond which statistical differences in texture features from DCE-MRI maps may occur. Indeed, even if temporal resolution had an influence on several texture features, post-hoc tests with correction for multiple comparisons showed that data with temporal resolution below 8s could be pooled, as well as data with temporal resolution above 8s. On the contrary, we found that data obtained with a scan duration of 5min should not be pooled with those with a scan duration of 3 or 4min.

After correction of multiple tests, some radiomics features extracted from AUC and  $K^{\text{trans}}$  maps demonstrated linear relationships with sampling. All belonged to the GLSZM category. `GLSZM_Size_zone_non_uniformity` and `GLSZM_Grey_level_non_uniformity` increased with downsampling, suggesting more heterogeneity in intensity values and in size zone volumes of the same grey level voxels with low temporal resolutions (high dt). Conversely, `GLSZM_Large_area_emphasis` and `GLSZM_Zone_variance` tended to decrease, suggesting that poor temporal resolution (high dt) led to smaller size zones. No linear correlation was found with truncating, probably because we only generated 3 time points. Poor temporal resolution (high dt) can be responsible for less accurate estimations, especially when the tumor – or areas in the tumor – demonstrates a rapid and strong enhancement (wash-in and peak on time-intensity curves). Consequently, hypervascularized intra-tumoral areas with high  $K^{\text{trans}}$  and AUC values could be missed, resulting in areas with lower values of  $K^{\text{trans}}$  and AUC.

All the categories of texture features seemed equally influenced by temporal resolution, but the dispersion was more marked with FOS, then GLCM, GLRLM and finally GLSZM. The high sensitivity of FOS could be due to their lack of spatial information. Indeed, all the voxels are pooled without considering the fact that

adjacent voxels may react similarly and proportionally to changes in temporal parameters, which is the case of GLCM, GLSZM and GLRLM.

Regarding the influence of temporal parameters on the performance of a model for response prediction based on AUC and  $K^{\text{trans}}$  of STS, we identified 6 relevant features that were selected across the different models, namely: FOS\_Inter\_quartile\_range, FOS\_Standard\_deviation, GLCM\_Correlation, GLRLM\_Long\_run\_emphasis, GLRLM\_Run\_entropy and GLSZM\_Small\_area\_emphasis. Interestingly, GLRLM\_Run\_entropy and GLRLM\_Small\_area\_emphasis were not significantly influenced by temporal resolution and showed low CVs. Thus, these texture features could be good candidates for multi-center studies based on DCE-MRI sequences of STS. However, these results do not mean that ultra-fast DCE-MRI acquisitions are unnecessary. The aim of DCE-MRI is to represent and estimate at best the vascular characteristics of tumors. Hypervascularized tumors require excellent temporal resolutions. If some researchers want to increase the statistical power of their radiomics study by putting together DCE-MRIs with different temporal parameters, then it should be carefully done because it could introduce a significant bias in their results.

We did not investigate the test-retest reproducibility of DCE-MRI-based texture features because it was hardly justifiable to inject a contrast agent twice in cancer patients. However, further radiomics studies performed on perfusion phantoms could help analyzing this crucial aspect. It should be noted that we designed our study to limit bias that could have been introduced in the quantification of heterogeneity: we utilized the same 1.5T MR-system, the same DCE-MRI sequences with the same acquisition parameters following QIBA® recommendations, the same contrast agent, the same imaging filters, the same software for post-processing and the same feature extraction parameters. Nevertheless, we had to adjust the coils because of variations in tumor sizes and locations, which may have introduced some bias. Moreover, truncating and downsampling the AIFs probably contributed to the variations in texture features from DCE-MRI parametric maps, even if we kept the same voxels in the same artery of interest. Indeed, the AIF is crucial in pharmacokinetic modeling (31). For instance, a recent study showed that  $K^{\text{trans}}$  could range from 0.25/min to more 2/min in prostate cancers in a same series of DCE-MRI acquisitions depending on the method to determine the AIF from different cancer centers, which led to variations in times to peak and peak amplitudes (39). Herein, poor temporal

resolutions could lead to missing the real AIF peak though the  $K^{\text{trans}}$  estimation strongly relies on it, as well as to superposition of the AIF and the tumor enhancement curve during the first part of the acquisition.

Our study has several limits. First, the population was small and made of heterogeneous histological types, though all were high-grade. Some tumors enhanced rather homogeneously and progressively (for instance myxoid/round cell liposarcomas) while others showed more heterogeneous enhancements, with the time-intensity curves of some components displaying a strong wash-in, followed by a peak and a wash-out (for instance, undifferentiated pleomorphic sarcomas). Temporal parameters were certainly more influential in the second case. Nevertheless, until now, the inclusion of STS patients in clinical trials relies on tumor grade and not on histotypes. Second, we did not investigate other semi-quantitative and pharmacokinetic DCE-MRI parameters (such as Time-to-peak, Wash-in, Wash-out,  $K^{\text{ep}}$  [efflux rate constant from the extra-cellular, extra-vascular space to the plasma compartment],  $K^{\text{el}}$  [contrast agent elimination rate constant],  $V_e$  [extra-cellular, extra-vascular space volume],  $V_p$  [plasmatic volume]), or other perfusion models than extended Tofts. We decided to focus on the most studied parameters in the literature. However, given that some areas in STS can show a wash-out, it is also possible that the pharmacokinetics that quantify the decreasing part of the time-intensity curve are also influenced by temporal parameters. Third, alternative methods for downsampling could have been applied by recombining k-space data instead of removing some phases (38). In a clinical setting, there is a compromise between temporal resolution, signal-to-noise ratio and spatial resolution. A decrease in temporal resolution will benefit signal-to-noise-ratio (by averaging twice if there is a down-sampling by a factor 2, for instance). Fourth, our multivariate models for the outcome sub-study can be questioned since only 20 patients were included with 2 definitions of good treatment responses depending on the patient's operability. We used a classical statistical approach without validation cohort to build the predictive models. More advanced selection methods could have been used (for instance: least absolute shrinkage and selection operator, ElasticNet, supervised principal component analysis), as well as supervised machine-learning classifiers (for instance: random forest, k-nearest neighbors, support vector machines) or deep learning (40).

Consequently, we did not test if the influence of temporal parameters was still present with these other statistical methods. The aim of this part of the study was to illustrate the influence of temporal parameters on a prediction and not to validate a radiomics model for response prediction. However, we hope that further prospective studies will take into account this research aiming at improving the quality of radiomics methods in order to build clean and robust models to answer key oncological questions.

To conclude, our study screened several aspects of the influence of temporal parameters on texture features extracted from DCE-MRI parametric maps of STS. We showed that both scan duration and temporal resolution introduced a non-negligible variability in the quantification of heterogeneity that could lead to a decreased performance of prediction models for response to chemotherapy. In addition to all the other acquisition and post-processing parameters, standardizing the scan duration and temporal resolution of DCE-MRI must be considered in prospective multi-centric trials to build reliable radiomics approaches.

## REFERENCES

1. O'Connor JPB: Cancer heterogeneity and imaging. *Semin Cell Dev Biol* 2017; 64:48–57.
2. Limkin EJ, Sun R, Dercle L, et al.: Promises and challenges for the implementation of computational medical imaging (radiomics) in oncology. *Ann Oncol* 2017; 28:1191–1206.
3. Jackson A, O'Connor JPB, Parker GJM, Jayson GC: Imaging tumor vascular heterogeneity and angiogenesis using dynamic contrast-enhanced magnetic resonance imaging. *Clin Cancer Res* 2007; 13:3449–3459.
4. O'Connor JPB, Aboagye EO, Adams JE, et al.: Imaging biomarker roadmap for cancer studies. *Nat Rev Clin Oncol* 2017; 14:169–186.
5. Ginsburg SB, Algohary A, Pahwa S, et al.: Radiomic features for prostate cancer detection on MRI differ between the transition and peripheral zones: Preliminary findings from a multi-institutional study. *J Magn Reson Imaging* 2017; 46:184–193.
6. Nie K, Shi L, Chen Q, et al.: Rectal Cancer: Assessment of Neoadjuvant Chemoradiation Outcome based on Radiomics of Multiparametric MRI. *Clin Cancer Res* 2016; 22:5256–5264.
7. Braman NM, Etesami M, Prasanna P, et al.: Intratumoral and peritumoral radiomics for the pretreatment prediction of pathological complete response to neoadjuvant chemotherapy based on breast DCE-MRI. *Breast Cancer Res* 2017; 19:57.
8. Bowen SR, Yuh WTC, Hippe DS, et al.: Tumor radiomic heterogeneity: Multiparametric functional imaging to characterize variability and predict response following cervical cancer radiation therapy. *J Magn Reson Imaging* 2018; 47:1388–1396.
9. Liu C, Ding J, Spuhler K, et al.: Preoperative prediction of sentinel lymph node metastasis in breast cancer by radiomic signatures from dynamic contrast-enhanced MRI. *J Magn Reson Imaging* 2019; 49:131–140.
10. Thomassin-Naggara I, Soualhi N, Balvay D, Darai E, Cuenod C-A: Quantifying tumor vascular heterogeneity with DCE-MRI in complex adnexal masses: A preliminary study. *J Magn Reson Imaging* 2017; 46:1776–1785.
11. Fan M, Cheng H, Zhang P, et al.: DCE-MRI texture analysis with tumor subregion partitioning for predicting Ki-67 status of estrogen receptor-positive breast cancers. *J Magn Reson Imaging* 2018; 48:237–247.
12. Rose CJ, Mills SJ, O'Connor JPB, et al.: Quantifying spatial heterogeneity in dynamic contrast-enhanced MRI parameter maps. *Magn Reson Med* 2009; 62:488–499.
13. Zhao F, Ahlawat S, Farahani SJ, et al.: Can MR imaging be used to predict tumor grade in soft-tissue sarcoma? *Radiology* 2014; 272:192–201.
14. Soldatos T, Ahlawat S, Montgomery E, Chalian M, Jacobs MA, Fayad LM: Multiparametric Assessment of Treatment Response in High-Grade Soft-Tissue Sarcomas with Anatomic and Functional MR Imaging Sequences. *Radiology* 2016; 278:831–840.
15. Meyer JM, Perlewitz KS, Hayden JB, et al.: Phase I trial of preoperative chemoradiation plus sorafenib for high-risk extremity soft tissue sarcomas with dynamic contrast-enhanced MRI correlates. *Clin Cancer Res* 2013; 19:6902–6911.
16. Cromb e A, Le Loarer F, Cornelis F, et al.: High-grade soft-tissue sarcoma: optimizing injection improves MRI evaluation of tumor response. *Eur Radiol* 2019; 29:545–555.

17. Huang W, Beckett BR, Tudorica A, et al.: Evaluation of Soft Tissue Sarcoma Response to Preoperative Chemoradiotherapy Using Dynamic Contrast-Enhanced Magnetic Resonance Imaging. *Tomography* 2016; 2:308–316.
18. Tian F, Hayano K, Kambadakone AR, Sahani DV: Response assessment to neoadjuvant therapy in soft tissue sarcomas: using CT texture analysis in comparison to tumor size, density, and perfusion. *Abdom Imaging* 2015; 40:1705–1712.
19. Hayano K, Tian F, Kambadakone AR, et al.: Texture Analysis of Non-Contrast-Enhanced Computed Tomography for Assessing Angiogenesis and Survival of Soft Tissue Sarcoma. *J Comput Assist Tomogr* 2015; 39:607–612.
20. Buch K, Kuno H, Qureshi MM, Li B, Sakai O: Quantitative variations in texture analysis features dependent on MRI scanning parameters: A phantom model. *J Appl Clin Med Phys* 2018; 19:253–264.
21. Mayerhoefer ME, Szomolanyi P, Jirak D, Materka A, Trattnig S: Effects of MRI acquisition parameter variations and protocol heterogeneity on the results of texture analysis and pattern discrimination: an application-oriented study. *Med Phys* 2009; 36:1236–1243.
22. Collewet G, Strzelecki M, Mariette F: Influence of MRI acquisition protocols and image intensity normalization methods on texture classification. *Magn Reson Imaging* 2004; 22:81–91.
23. Ford J, Dogan N, Young L, Yang F: Quantitative Radiomics: Impact of Pulse Sequence Parameter Selection on MRI-Based Textural Features of the Brain. *Contrast Media Mol Imaging* 2018; 2018:1729071.
24. Othman AE, Falkner F, Martirosian P, et al.: Optimized Fast Dynamic Contrast-Enhanced Magnetic Resonance Imaging of the Prostate: Effect of Sampling Duration on Pharmacokinetic Parameters. *Invest Radiol* 2016; 51:106–112.
25. Othman AE, Falkner F, Weiss J, et al.: Effect of Temporal Resolution on Diagnostic Performance of Dynamic Contrast-Enhanced Magnetic Resonance Imaging of the Prostate. *Invest Radiol* 2016; 51:290–296.
26. Hao W, Zhao B, Wang G, Wang C, Liu H: Influence of scan duration on the estimation of pharmacokinetic parameters for breast lesions: a study based on CAIPIRINHA-Dixon-TWIST-VIBE technique. *Eur Radiol* 2015; 25:1162–1171.
27. Bogowicz M, Riesterer O, Bundschuh RA, et al.: Stability of radiomic features in CT perfusion maps. *Phys Med Biol* 2016; 61:8736–8749.
28. Cousin S, Crombe A, Stoeckle E, et al.: Clinical, radiological and genetic features, associated with the histopathologic response to neoadjuvant chemotherapy (NAC) and outcomes in locally advanced soft tissue sarcoma (STS) patients (pts). *JCO* 2017; 35(15\_suppl):11014–11014.
29. Ray-Coquard I, Collard O, Ducimetiere F, et al.: Treatment patterns and survival in an exhaustive French cohort of pazopanib-eligible patients with metastatic soft tissue sarcoma (STS). *BMC Cancer* 2017; 17:111.
30. Michaely HJ, Morelli JN, Budjan J, et al.: CAIPIRINHA-Dixon-TWIST (CDT)-volume-interpolated breath-hold examination (VIBE): a new technique for fast time-resolved dynamic 3-dimensional imaging of the abdomen with high spatial resolution. *Invest Radiol* 2013; 48:590–597.
31. Tofts PS, Brix G, Buckley DL, et al.: Estimating kinetic parameters from dynamic contrast-enhanced T(1)-weighted MRI of a diffusable tracer: standardized quantities and symbols. *J Magn Reson Imaging* 1999; 10:223–232.
32. Haralick RM, Shanmugam K, Dinstein I: Textural features of image classification. *IEEE Transactions on Systems, Man, & Cybernetics* 1973; 3:610–621.

33. Galloway MM: Texture analysis using gray level run lengths. *Computer Graphics and Image Processing* 1975; 4:172–179.
34. Thibault G, Fertil B, Navarro C, et al.: Texture Indexes and Gray Level Size Zone Matrix Application to Cell Nuclei Classification. 2009.
35. DeLong ER, DeLong DM, Clarke-Pearson DL: Comparing the areas under two or more correlated receiver operating characteristic curves: a nonparametric approach. *Biometrics* 1988; 44:837–845.
36. Vallières M, Freeman CR, Skamene SR, El Naqa I: A radiomics model from joint FDG-PET and MRI texture features for the prediction of lung metastases in soft-tissue sarcomas of the extremities. *Phys Med Biol* 2015; 60:5471–5496.
37. Kuhl CK, Mielcareck P, Klaschik S, et al.: Dynamic breast MR imaging: are signal intensity time course data useful for differential diagnosis of enhancing lesions? *Radiology* 1999; 211:101–110.
38. Heisen M, Fan X, Buurman J, van Riel NAW, Karczmar GS, ter Haar Romeny BM: The influence of temporal resolution in determining pharmacokinetic parameters from DCE-MRI data. *Magn Reson Med* 2010; 63:811–816.
39. Huang W, Chen Y, Fedorov A, et al.: The Impact of Arterial Input Function Determination Variations on Prostate Dynamic Contrast-Enhanced Magnetic Resonance Imaging Pharmacokinetic Modeling: A Multicenter Data Analysis Challenge. *Tomography* 2016; 2:56–66.
40. Erickson BJ, Korfiatis P, Akkus Z, Kline TL: Machine Learning for Medical Imaging. *Radiographics* 2017; 37:505–515.

**TABLE 1.** MRI texture features extracted from  $K^{\text{trans}}$  and AUC maps.

<b>First-order Feature</b>	<b>Grey level co-occurrence matrix</b>	<b>Grey level run length matrix</b>	<b>Grey level size zone matrix</b>
Average	Cluster prominence	GL non-uniformity	GL non-uniformity
Energy	Cluster shade	GL variance	GL variance
Entropy	Cluster tendency	High GL run emphasis	Large area emphasis
Inter-quartile range	Contrast	Low GL run emphasis	Small area emphasis
Kurtosis	Correlation	Long run emphasis	Size zone non-uniformity
Skewness	Inverse difference moment	Run entropy	Zone entropy
Standard deviation	Joint average	Run length non-uniformity	Zone variance
	Joint energy	Run variance	
	Joint entropy	Short run emphasis	

NOTE. Abbreviations: GL: grey level

**TABLE 2.** Epidemiological features of the population study.

<b>Characteristics</b>	<b>Patients</b>
<b>Gender</b>	
Men	16/25 (64%)
Women	9/25 (36%)
<b>Age (years)</b>	68 (31-94)
<b>Histological types</b>	
Undifferentiated pleomorphic sarcoma	13/25 (52%)
Myxoid/round cells liposarcoma	4/25 (16%)
Rhabdomyosarcoma	2/25 (8%)
Myxofibrosarcoma	1/25 (4%)
Synovial sarcoma	2/25 (8%)
Pleomorphic liposarcoma	1/25 (4%)
Undifferentiated sarcoma - others	2/25 (8%)
<b>Location</b>	
Upper limb	4/25 (16%)
Shoulder girdle	1/25 (4%)
Trunk wall	2/25 (8%)
Lower limb	18/25 (72%)
<b>Size (mm)</b>	81 (42-180)
<b>Number of voxels</b>	356 959 (22 816-1 048 136)
<b>Volume (L)</b>	0.357 (0.023-1.048)
<b>Tumor depth</b>	
Deep	16/25 (64%)
Deep and superficial	8/25 (32%)
Superficial	1/25 (4%)

NOTE. Data are number of patients with percentage in parentheses, except for age, size, number of voxels and volume of the tumor, given as median and range.

**TABLE 3.** Assessment of the influence of temporal resolution (sampling) and scan duration (truncating) on texture parameters extracted from DCE-MRI parametric maps ( $K^{trans}$  and AUC).

Texture features	AUC - Sampling		$K^{trans}$ - Sampling		$K^{trans}$ - Truncating	
	F-value	p-value	F-value	p-value	F-value	p-value
<b>First-order Feature</b>						
Average	18.54	<b>0.0050**</b>	5.12	0.5290	14.60	<b>0.0022**</b>
Energy	25.55	<b>0.0003***</b>	2.13	0.9072	15.00	<b>0.0018**</b>
Entropy	7.15	0.3069	16.46	<b>0.0115*</b>	19.19	<b>0.0002***</b>
Inter-quartile range	8.607	0.1969	5.61	0.4688	15.05	<b>0.0018**</b>
Kurtosis	50.89	<b>&lt;0.0001***</b>	6.35	0.0958	15.49	<b>0.0168*</b>
Skewness	41.57	<b>&lt;0.0001***</b>	10.88	0.0921	8.80	<b>0.0321*</b>
Standard deviation	26.12	<b>0.0002***</b>	1.77	0.9395	14.50	<b>0.0023**</b>
<b>GLCM</b>						
Cluster prominence	17.07	<b>0.0090**</b>	11.46	0.0751	16.20	<b>0.0010**</b>
Cluster shade	5.07	0.5354	12.15	0.0587	12.55	<b>0.0057**</b>
Cluster tendency	10.30	0.1127	9.96	0.1262	23.85	<b>&lt;0.0001***</b>
Contrast	9.27	0.1589	13.7	<b>0.0331*</b>	17.85	<b>0.0005***</b>
Correlation	2.78	0.8358	5.59	0.4709	4.25	0.2357
Inverse difference moment	6.58	0.3617	13.70	<b>0.0331*</b>	17.85	<b>0.0005***</b>
Joint average	1.94	0.9253	13.96	<b>0.0301*</b>	18.75	<b>0.0003***</b>
Joint energy	6.45	0.3750	13.83	<b>0.0316*</b>	18.40	<b>0.0004***</b>
Joint entropy	6.87	0.3327	16.64	<b>0.0233*</b>	19.55	<b>0.0002***</b>
<b>GLRLM</b>						
GL non-uniformity	0.96	0.9869	5.83	0.4427	1.05	0.7892
GL variance	20.74	<b>0.0020**</b>	17.7	<b>0.0070*</b>	29.30	<b>&lt;0.0001***</b>
High GL run emphasis	5.74	0.4525	19.16	<b>0.0039**</b>	29.30	<b>&lt;0.0001***</b>
Low GL run emphasis	3.27	0.7746	19.16	<b>0.0039**</b>	29.30	<b>&lt;0.0001***</b>
Long run emphasis	11.00	0.0884	17.05	<b>0.0091**</b>	31.50	<b>&lt;0.0001***</b>
Run entropy	0.32	0.8632§	1.40	0.2556§	0.9251	0.4056§
Run length non-uniformity	7.32	0.2918	11.46	0.0753	14.85	<b>0.0019**</b>
Run variance	10.47	0.1062	11.36	0.0778	5.95	0.1141
Short run emphasis	13.23	<b>0.0395*</b>	1.56	0.2133	22.95	<b>&lt;0.0001***</b>
<b>GLSZM</b>						
GL non-uniformity	9.69	0.1384	15.31	<b>0.0180*</b>	10.94	0.012
GL variance	25.72	<b>0.0003***</b>	11.89	0.0645	10.18	0.0171
Large area emphasis	19.29	<b>0.0037**</b>	21.41	<b>0.0015**</b>	15.30	<b>0.0016**</b>
Small area emphasis	9.16	0.1649	4.91	0.5555	4.40	0.2214
Size zone non-uniformity	16.11	<b>0.0132*</b>	16.87	<b>0.0098*</b>	5.87	0.118
Zone entropy	3.08	0.2190§	4.746	0.5768	1.01	0.3797§
Zone variance	20.26	<b>0.0025**</b>	23.46	<b>0.0007***</b>	15.30	<b>0.0016**</b>

NOTE. Data are F-values and p-values for the repeated measures (rm-) ANOVA (: §) or non parametric equivalent rm-Friedman test.

Abbreviations: GL : grey-level; GLCM : grey-level occurrence matrix; GLRLM: grey-level run length matrix; GLSZM: grey level size zone matrix

\*:  $p \leq 0.05$ ; \*\*:  $p < 0.005$ , \*\*\*:  $p < 0.001$

**TABLE 4.** Summary of the post-hoc tests: number of texture features that were significantly different when comparing 2 distinct temporal resolution (: sampling) for AUC **(a)** and  $K^{trans}$  **(b)**, or 2 distinct scan durations (: truncating) for  $K^{trans}$  **(c)**.

**a. AUC - Sampling**

	dt2	dt4	dt6	dt8	dt10	dt12	dt20
dt2	-	0	0	2	4	1	10
dt4	0	-	0	2	2	0	9
dt6	0	0	-	0	0	0	2
dt8	2	2	0	-	0	0	0
dt10	4	2	0	0	-	0	0
dt12	1	0	0	0	0	-	0
dt20	10	9	2	0	0	0	-

**b.  $K^{trans}$  - Sampling**

	dt2	dt4	dt6	dt8	dt10	dt12	dt20
dt2	-	0	0	0	0	0	10
dt4	0	-	0	0	0	0	2
dt6	0	0	-	0	0	0	6
dt8	0	0	0	-	0	0	0
dt10	0	0	0	0	-	0	0
dt12	0	0	0	0	0	-	0
dt20	10	2	6	0	0	0	-

**c.  $K^{trans}$  - Truncating**

	T3'00	T4'00	T5'00
T3'00	-	0	17
T4'00	0	-	23
T5'00	17	23	-

NOTE. Abbreviations: dtx corresponds to a sampling of 'x' seconds; Ty corresponds to a scan duration of 'y' minutes.

**TABLE 5.** Degree of dispersion of the texture features from  $K^{trans}$  and AUC maps according to temporal resolution (: sampling) and scan duration (: truncating).

	<b>Very poorly variable</b> <b>CV &lt; 0.10</b>	<b>Poorly variable</b> <b>0.10 ≤ CV &lt; 0.20</b>	<b>Mildly variable</b> <b>0.20 ≤ CV &lt; 0.50</b>	<b>Highly variable</b> <b>0.50 ≤ CV ≤ 1</b>	<b>Extremely variable</b> <b>CV ≥ 1.00</b>
<b>AUC - Sampling</b>	GLCM_Inverse Difference Moment	FOS_Average	FOS_Energy	GLCM_Cluster prominence	
	GLCM_Joint average	FOS_Inter-quartile range	FOS_Entropy		
	GLCM_Joint energy	FOS_Standard deviation	FOS_Kurtosis		
	GLRLM_GL non-uniformity	GLRLM_Low GL run emphasis	FOS_Skewness		
	GLRLM_High GL run emphasis	GLRLM_Long run emphasis	GLCM_Cluster shade		
	GLRLM_Run length non-uniformity	GLSZM_Small area emphasis	GLCM_Cluster tendency		
	GLRLM_Run entropy	GLSZM_Zone entropy	GLCM_Correlation		
	GLRLM_Run variance		GLCM_Contrast		
	GLRLM_Short run emphasis		GLCM_Joint entropy		
			GLRLM_GL variance		
		GLSZM_GL non-uniformity			
		GLSZM_GL variance			
		GLSZM_Large area emphasis			
		GLSZM_Zone variance			
		GLSZM_Size zone non-uniformity			
<b><math>K^{trans}</math> - Sampling</b>	GLCM_Inverse Difference Moment	GLRLM_Run variance	FOS_Entropy	FOS_Inter-quartile range	FOS_Energy
	GLCM_Joint average	GLRLM_Short run emphasis	GLCM_Correlation	FOS_Kurtosis	
	GLCM_Joint energy	GLSZM_Small area emphasis	GLRLM_GL variance	FOS_Average	
	GLRLM_GL non-uniformity	GLSZM_Zone entropy	GLRLM_Long run emphasis	FOS_Skewness	
	GLRLM_High GL run emphasis		GLRLM_Run length non-uniformity	FOS_Standard deviation	
	GLRLM_Low GL run emphasis		GLSZM_GL non-uniformity	GLCM_Cluster prominence	
	GLRLM_Run entropy		GLSZM_GL variance	GLCM_Cluster shade	
			GLSZM_Large area emphasis	GLCM_Cluster tendency	
			GLSZM_Zone variance	GLCM_Contrast	
			GLSZM_Size zone non-uniformity	GLCM_Joint entropy	
<b><math>K^{trans}</math> - Truncating</b>	GLCM_Inverse Difference Moment	GLRLM_Long run emphasis	FOS_Entropy	FOS_Average	
	GLCM_Joint average	GLRLM_Run length non-uniformity	FOS_Kurtosis	FOS_Energy	
	GLCM_Joint energy	GLRLM_Run variance	FOS_Skewness	FOS_Inter-quartile range	
	GLRLM_GL non-uniformity	GLSZM_Small area emphasis	GLCM_Cluster prominence	FOS_Standard deviation	
	GLRLM_High GL run emphasis		GLCM_Cluster shade	GLSZM_Zone entropy	
	GLRLM_Low GL run emphasis		GLCM_Cluster tendency		
	GLRLM_Run entropy		GLCM_Correlation		
	GLRLM_Short run emphasis		GLCM_Contrast		
			GLCM_Joint entropy		
			GLRLM_GL variance		
		GLSZM_GL non-uniformity			
		GLSZM_GL variance			
		GLSZM_Large area emphasis			
		GLSZM_Zone variance			
		GLSZM_Size zone non-uniformity			

NOTE. Abbreviations: CV: coefficient of variation; FOS: First order statistics; GL: grey level; GLCM: grey level co-occurrence matrix; GLRLM: grey level run length matrix; GLSZM: grey level size zone matrix

**TABLE 6.** Area under the ROC curves of models for response prediction to chemotherapy based on texture features extracted from AUC and  $K^{\text{trans}}$  maps with varying temporal resolution (sampling) and scan duration (truncating)

Temporal parameters	Univariate analysis		Model	
	Significant features	p-value	AUROC (CI95%)	p-value
<b>◆ Sampling</b>				
<b>dt2</b>	$K^{\text{trans}}$ _GLRLM_Run entropy	0.021	0.85 (0.68-1.00)	0.021
	AUC_GLRLM_Run entropy	0.050		
<b>dt4</b>	AUC_GLRLM_Run entropy	0.050	0.84 (0.62-1.00)	0.026
	$K^{\text{trans}}$ _FOS_Inter-quartile range	0.026		
	$K^{\text{trans}}$ _FOS_Standard deviation	0.013		
	$K^{\text{trans}}$ _GLRLM_Long run emphasis	0.021		
	$K^{\text{trans}}$ _GLRLM_Run entropy	0.032		
<b>dt6</b>	AUC_GLRLM_Run entropy	0.050	0.77 (0.54-1.00)	0.074
<b>dt8</b>	AUC_GLCM_Correlation	0.032	0.83 (0.61-1.00)	0.032
<b>dt10</b>	$K^{\text{trans}}$ _GLRLM_Long run emphasis	0.032	0.83 (0.63-1.00)	0.032
<b>dt12</b>	AUC_GLCM_Correlation	0.040	0.83 (0.58-1.00)	0.032
	AUC_GLRLM_Run entropy	0.032		
	$K^{\text{trans}}$ _GLSZM_Small area emphasis	0.050		
<b>dt20</b>	AUC_GLRLM_Run entropy	0.049	0.81 (0.58-1.00)	0.121
<b>◆ Truncating</b>				
<b>T3'00</b>	AUC_GLRLM_Run entropy	0.050	0.88 (0.71-1.00)	0.021
	$K^{\text{trans}}$ _GLSZM_Small area emphasis	0.021		
<b>T4'00</b>	AUC_GLRLM_Run entropy	0.050	0.90 (0.74-1.00)	0.018
	$K^{\text{trans}}$ _GLSZM_Small area emphasis	0.016		
<b>T5'00</b>	AUC_GLRLM_Run entropy	0.050	0.77 (0.54-1.00)	0.074

NOTE. Abbreviations: AUROC: area under the receiver operating characteristics curve; CI95%: 95% confidence interval; GL: grey level; GLCM: grey level co-occurrence matrix; GLRLM: grey level run length matrix; GLSZM: grey level size zone matrix; 'dtx' corresponds to a sampling of 'x' seconds; 'Ty' corresponds to a scan duration of 'y' minutes.

## FIGURE LEGENDS

**FIGURE 1: Reconstruction of data acquisition.** (a) Retrospective downsampling and truncating were performed to obtain post-processed data with a temporal resolution of 2s (: dt2), 4s (: dt4), 6s (: dt6s)... and 20s (: dt20), and with a scan duration of 4min (: T4'00 – with a temporal resolution of 6s) and 3min (: T3'00 - with a temporal resolution of 6s). Of note, the baseline was not re-sampled. (b) The same voxels in the same artery were used to determine the artery input function (AIF) that was used in the extended Tofts model. However, AIFs were also truncated and downsampled leading to variations in time to reach the peak (from 36s to 54s) and in maximum signal intensity of the peak (from 319 to 396.8) in this example of high-grade synovial sarcoma of the popliteal region. (c) Next, parametric maps of  $K^{\text{trans}}$  (: influx volume transfer constant) and (d) AUC (: area under the time intensity curves at 90s after arrival of the contrast agent bolus in the acquisition volume) were generated as functions of 'dt' and 'T'.

**FIGURE 2: Linear correlations between texture features from DCE-MRI parametric maps and temporal resolution.** Only significant correlations for AUC (a) and  $K^{\text{trans}}$  (b) after corrections to allow multiple comparisons are shown with their p-value. Sampling is given in seconds. Texture features have arbitrary units. Abbreviations: GL: grey level; GLSLZM: grey level size zone matrix.

**FIGURE 3: Illustrated case of the influence of temporal parameters on DCE-MRI parametric maps and texture features of sarcoma.** A 63 years old male with a high-grade, deep and superficial, myxofibrosarcoma of the left thigh underwent his baseline MRI examination including conventional sequences (a) and DCE-MRI acquisition. (b) The whole tumor volume was manually segmented, slice-by-slice, on the last phase of the DCE-MRI acquisition, i.e. 300s after Gadolinium chelates intravenous injection. (c) The AUC (: area under the time intensity curve at 90s after arrival of the contrast agent bolus in the acquisition volume, units: mmol/L/s, on the right) and  $K^{\text{trans}}$  (influx volume transfer constant, units: /s, on the left) parametric maps were reconstructed with the different scan durations and temporal resolutions. After the whole tumor volume segmentation, frequency histograms were reconstructed for (d) AUC depending on the different temporal resolution, (e)  $K^{\text{trans}}$  depending on the different temporal resolution, and (f)  $K^{\text{trans}}$  according to the

different scan duration. Abbreviation: STIR T2-WI: short time inversion recovery T2-weighted imaging, T2-WI: T2 weighted imaging; FS CE-T1-WI: fat saturation contrast enhanced T1 weighted imaging; DCE-MRI t=300s: last phase of the dynamic contrast enhanced MRI, on which was segmented the tumor volume, 'dtx' corresponds to a sampling of 'x' seconds; 'Ty' corresponds to a scan duration of 'y' minutes.

**FIGURE 4 Coefficient of variation of the texture features extracted from DCE-MRI depending on temporal parameters.** Influence of the temporal resolution of DCE-MRI acquisition (: sampling) on the dispersion of each texture feature from (a) AUC (: area under the time intensity curve) and (b)  $K^{\text{trans}}$  (: influx volume transfer constant) maps. (c) Influence of the scan duration (: truncating) on the dispersion of each texture feature extracted from  $K^{\text{trans}}$  map. Results are given with standard deviation. GL: grey level.

#### **SUPPLEMENTARY DATA**

**Supplementary Data 1.** Definition of the texture features

**Supplementary Data 2.** Assessment of linear correlations of all the texture features with a significant influence of temporal parameters according to repeated measures ANOVA (or non-parametric equivalent).

**Supplementary Data 3.** Coefficient of variations with standard deviation of all the texture features.

**Supplementary Data 4.** Univariate analysis of the associations between texture features and responses to chemotherapy for each model (depending on temporal resolution and scan duration).

**Supplementary Data 5.** Comparisons of the AUROC of the different models, depending on scan duration and temporal resolution

**FIGURE 1**

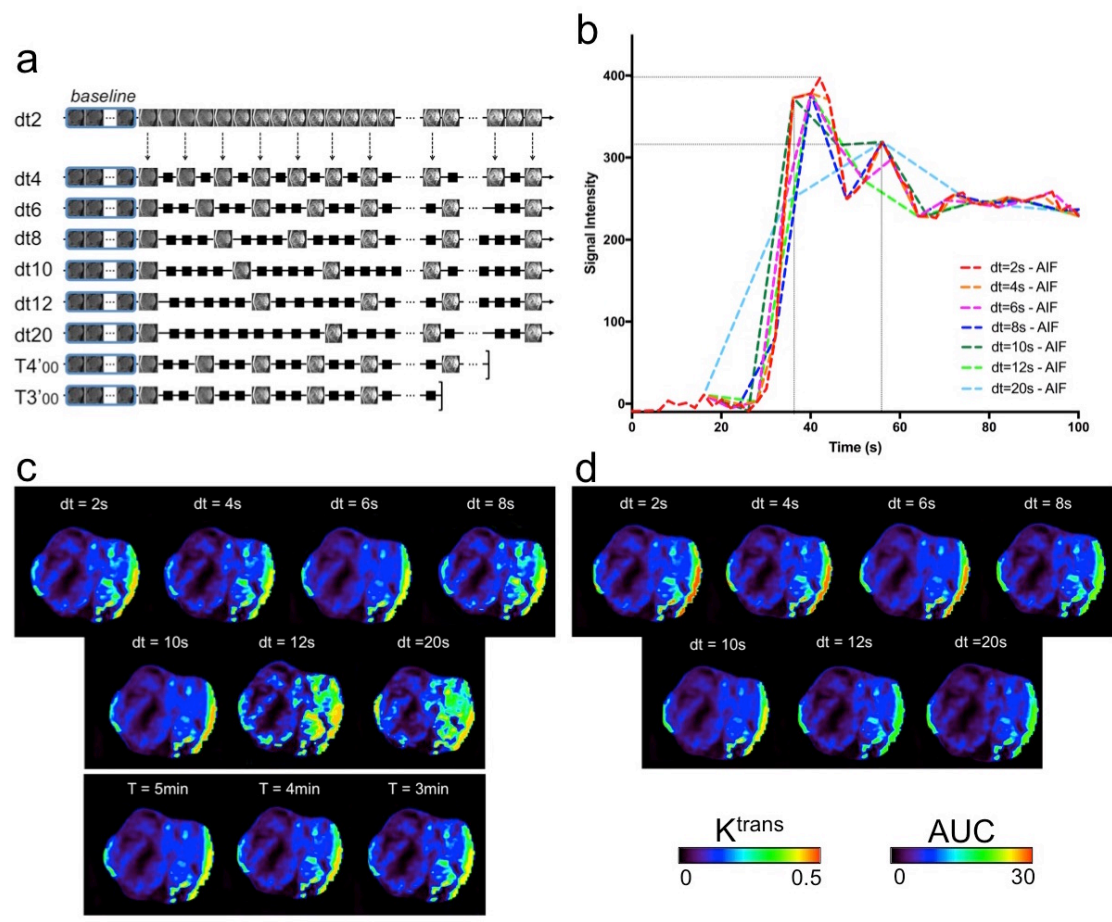
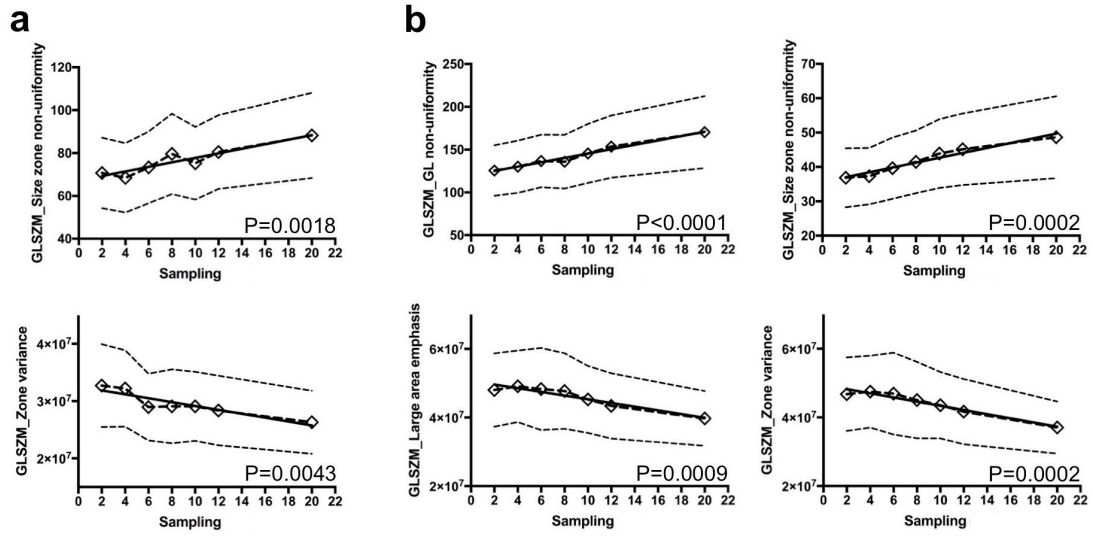


FIGURE 2.



**FIGURE 3.**

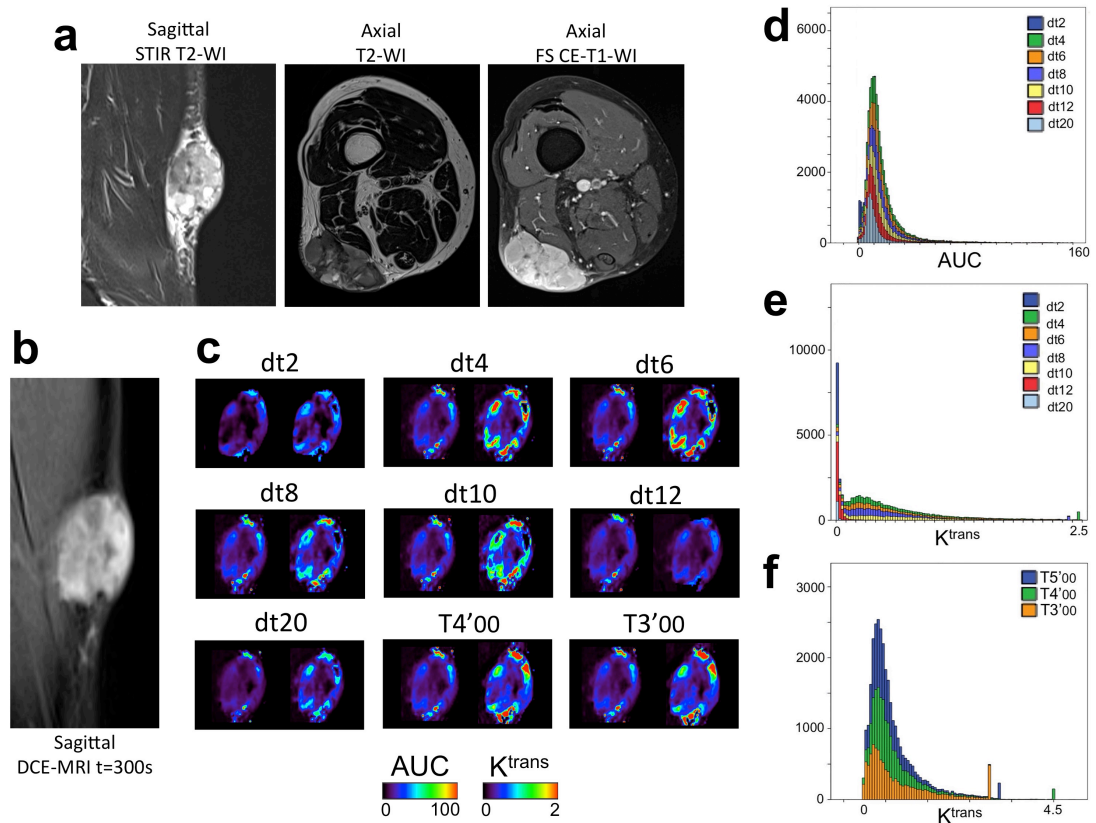


FIGURE 4.

